Atmospheric
Chemistry
and Physics

Open Access

EGU

Supplement of

Characterization of carbonaceous aerosols in Singapore: insight from black carbon fragments and trace metal ions detected by a soot particle aerosol mass spectrometer

Laura-Hélèna Rivellini et al.

Correspondence to: Alex King Yin Lee (ceelkya@nus.edu.sg)

Text S1: Effects of applying CDCE for rBC an OA on the PMF results

In this work, a constant collection efficiency (CE) of 0.6 was applied to determine refractory black carbon (rBC) mass concentrations (Willis et al., 2014). To evaluate the potential impacts of applying chemical dependent-collection efficiency (CDCE) correction for rBC and organic aerosol (OA) on the PMF results, we first determined the CDCE of rBC by comparing the BC concentrations (denoted as BC_{AE33}) measured by an aethalometer (AE33, Magee Scientific) and the EC mass concentrations measured by a semi-continuous OC/EC analyser (Sunset Laboratory). Comparisons between mass concentrations of our CE-corrected rBC ($rBC_{CE=0.6}$) with BC_{AE33} and EC give good Pearson coefficients of 0.96 and 0.71 and slopes of 0.83 and 1.10, respectively (Figure S3c and d). The histogram of CDCE determined for rBC using the two co-located instruments are reported in Figure S2b and c. The logarithmic distributions are centred on ~0.52 (±0.18) for aethalometer-based CDCE ($CDCE_{AE33}$) and 0.69 (±0.34) for OC/EC-based CDCE ($CDCE_{ECOC}$). Three additional PMF analysis were performed by applying CDCE for rBC and/or OA, while other PMF setting remains unchanged. The metal ion signals were corrected to nitrate equivalent mass concentrations by assuming their RIE values equal to 1.

- Laser-off OA corrected by CDCE that were calculated based on the approach described by Middlebrook et al., (2012) ($CDCE_{Mid}$)
- Laser-on $CDCE_{Mid}$-corrected OA and $CDCE_{AE33}$-corrected C_n^+
- Laser-on $CDCE_{Mid}$-corrected OA and $CDCE_{AE33}$-corrected C_n^+ and metal ions

Comparisons between the CDCE-corrected results and the corresponding base cases reported in the main text (i.e., laser-off OA, laser-on OA + C_n^+ and laser-on OA + C_n^+ + metals) are shown in Table S4. Note that all PMF runs lead to five-factor solution (i.e., HOA, O-HOA, COA, LO-OOA and MO-OOA). Below is the brief summary of some major changes:

- OA fragments as PMF input: The time series of OA factors determined with $CDCE_{Mid}$ applied are similar to those without correction (i.e., Pearson coefficients > 0.91). Applying $CDCE_{Mid}$ correction result in 19-27% changes in the mass concentrations of each factor.

- OA, rBC and metals as PMF input: These modifications of PMF input do not make significant impacts on the relative contribution of each factor to the total OA and rBC. Except for the HOA factor, its contribution to the total rBC mass decreased from 44% to 33%. The C_1^+/C_3^+ ratios for MO-OOA are much more sensitive to CDCE corrections (i.e., increased from. 0.29-0.54 to 1.57-1.67) compared to other PMF factors. Even without applying CDCE correction, the C_1^+/C_3^+ ratios for MO-OOA varied between 0.29 and 0.54. Due to such large variations between cases, in addition to COA, no C_1^+/C_3^+ ratios were reported for MO-OOA in the main text.

- The CDCE corrections can affect the contributions of the five metals from each PMF factor to their total signals as shown in Table 1. The changes in the contributions of sodium and nickel from the LO-OOA and HOA factors to their total signals are relatively large compared to other metals and OA factors. It is important to emphasise that a few key observations remain unchanged: (1) K^+ and Rb^+ are strongly associated with MO-OOA, (2) V^+ is mainly associated with LO-OOA, and (3) Na^+ is associated with a few OA factors that are related to combustion emissions (i.e., LO-OOA, O-HOA, and HOA).

Overall, applying CDCE corrections for OA, rBC and metals do not result in substantial changes in our interpretations for most of the key observations. The discussion and conclusion developed based on the distribution of metals to different OA factors remains unchanged. Therefore, the original PMF results are used as a base case in our discussion in the main text. Table 1 shows the possible ranges of different parameters based on the results obtained from the CDCE-corrected PMF analysis. Table S4 summarizes the results of pre- and post-CDCE-corrected PMF analysis (Pre-CDCE: PMF solution obtained by the CDCE-corrected input matrices, Post-CDCE: PMF solution corrected by CDCE).
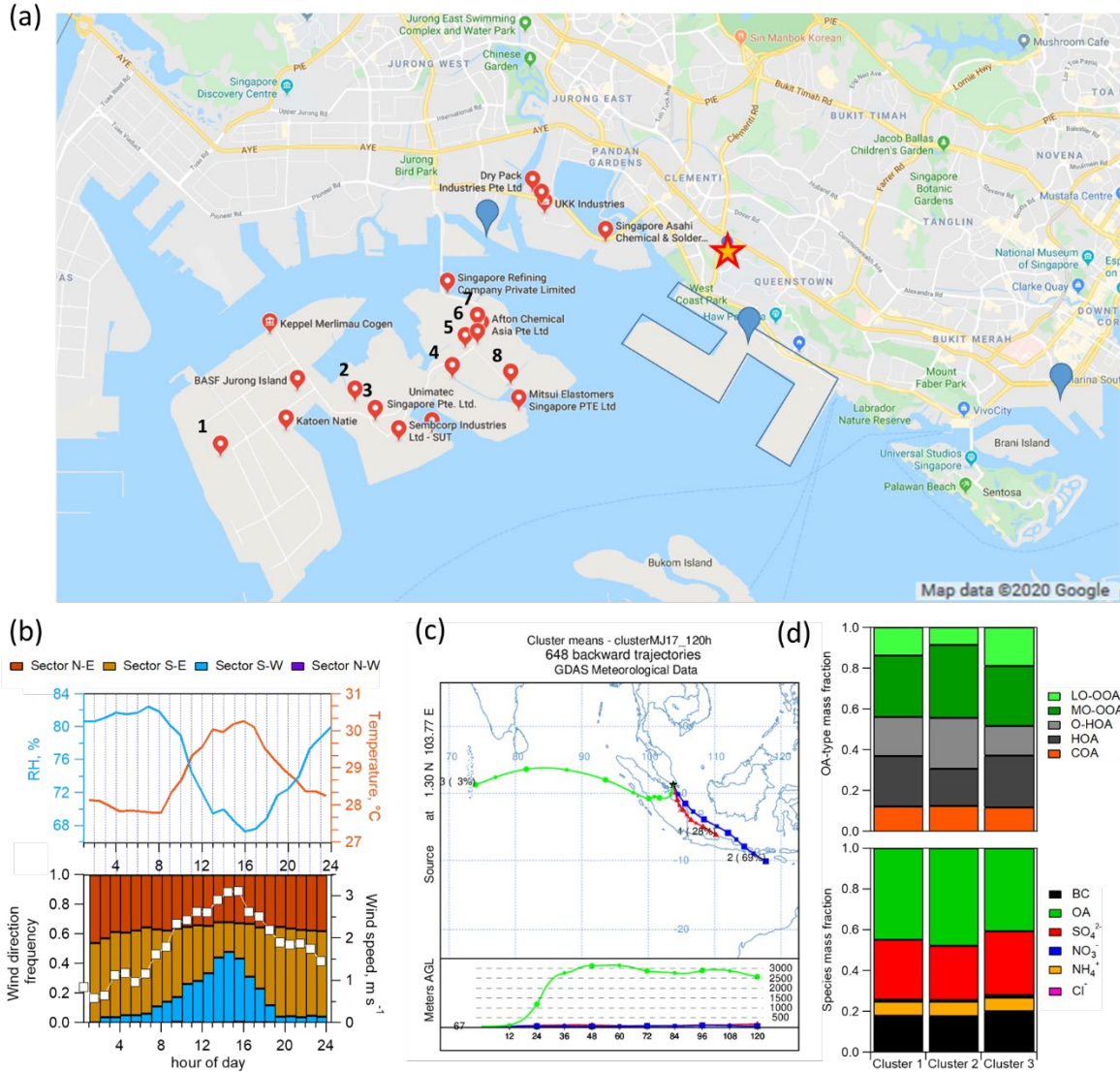
Figure S1: (a) Map overview of the measurement location (indicated by a star). The industrial areas (Tuas industrial estate and Jurong Island) are located in the southwest sector of the sampling site. The red pins and numbers indicate the following industries: (1) Evonik Methionine SEA, (2) ExxonMobil Chemical Plant, (3) Eastman Chemical, (4) Petrochemical Corporation of Singapore, (5) Linde Gas Singapore Pte Ltd, (6) SembCorp Industries Ltd, (7) Nouryon Surface Chemistry Pte Ltd, and (8) Shell Chemicals Seraya Pte Ltd. The blue pins and outlined areas represent the shipping ports. (b) Diurnal cycles of average RH (%), temperature (ºC), wind frequency per sector (N-E: 0-90°; S-E: 90-160°; S-W: 160-270°; N-W: 270-0°) and mean wind speed (m s^{-1}). (c) 3-cluster solution of air mass back-trajectories over the entire sampling period. (d) The average chemical compositions of PM$_1$ and OA for each back-trajectory cluster.
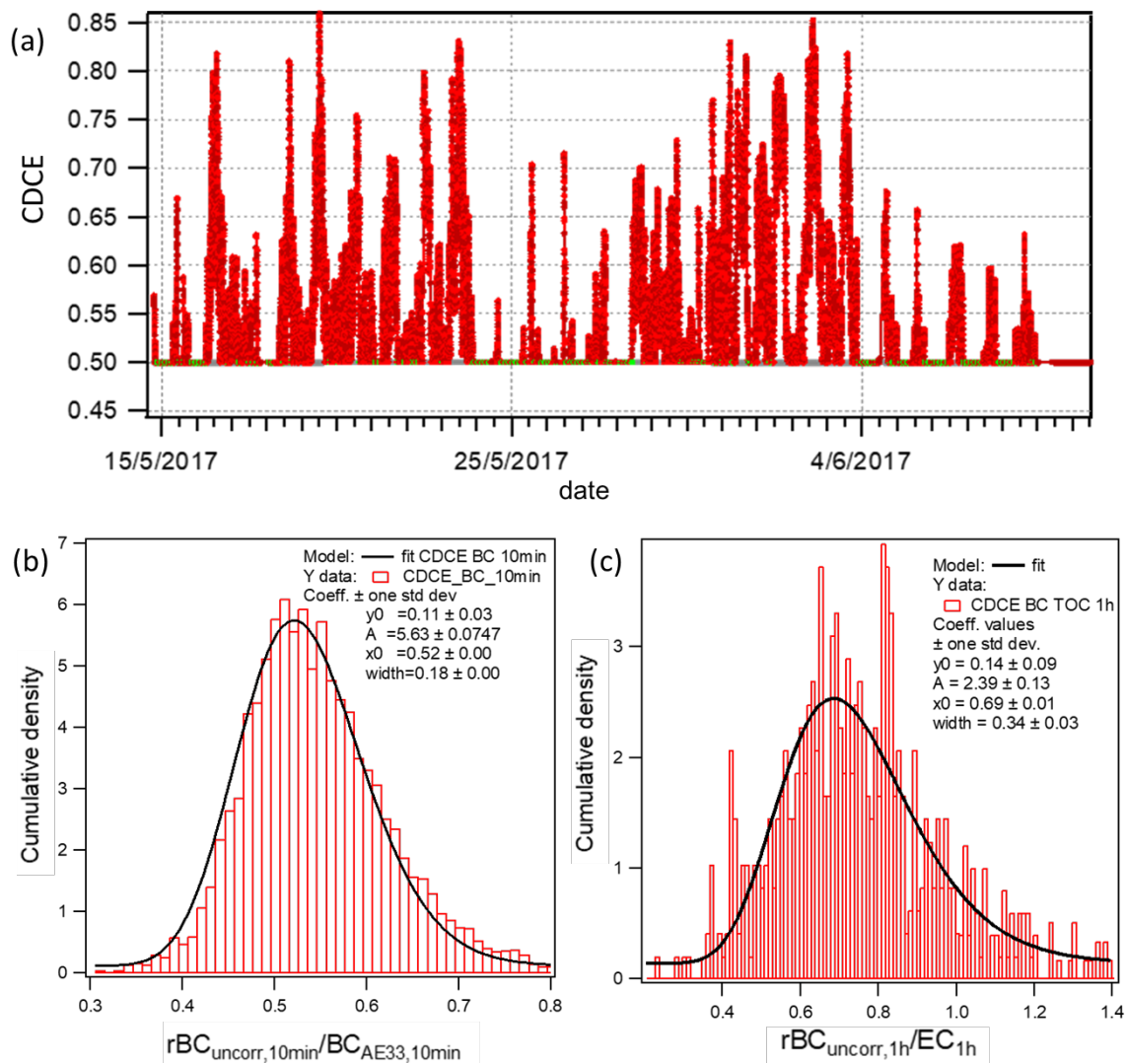
Figure S2: (a) Time series of composition-dependent collection efficiency (CDCE$_{Mid}$) determined over the entire campaign. Cumulative frequency of (b) aethalometer-based CDCE and (c) OC/EC-based CDCE, and their respective lognormal fitting determined over the entire campaign (with the fitting parameters corresponding to the following equation: $Y = y_0 + A \exp\left\{-\left[\frac{\ln(x/x_0)}{width}\right]^2\right\}$).
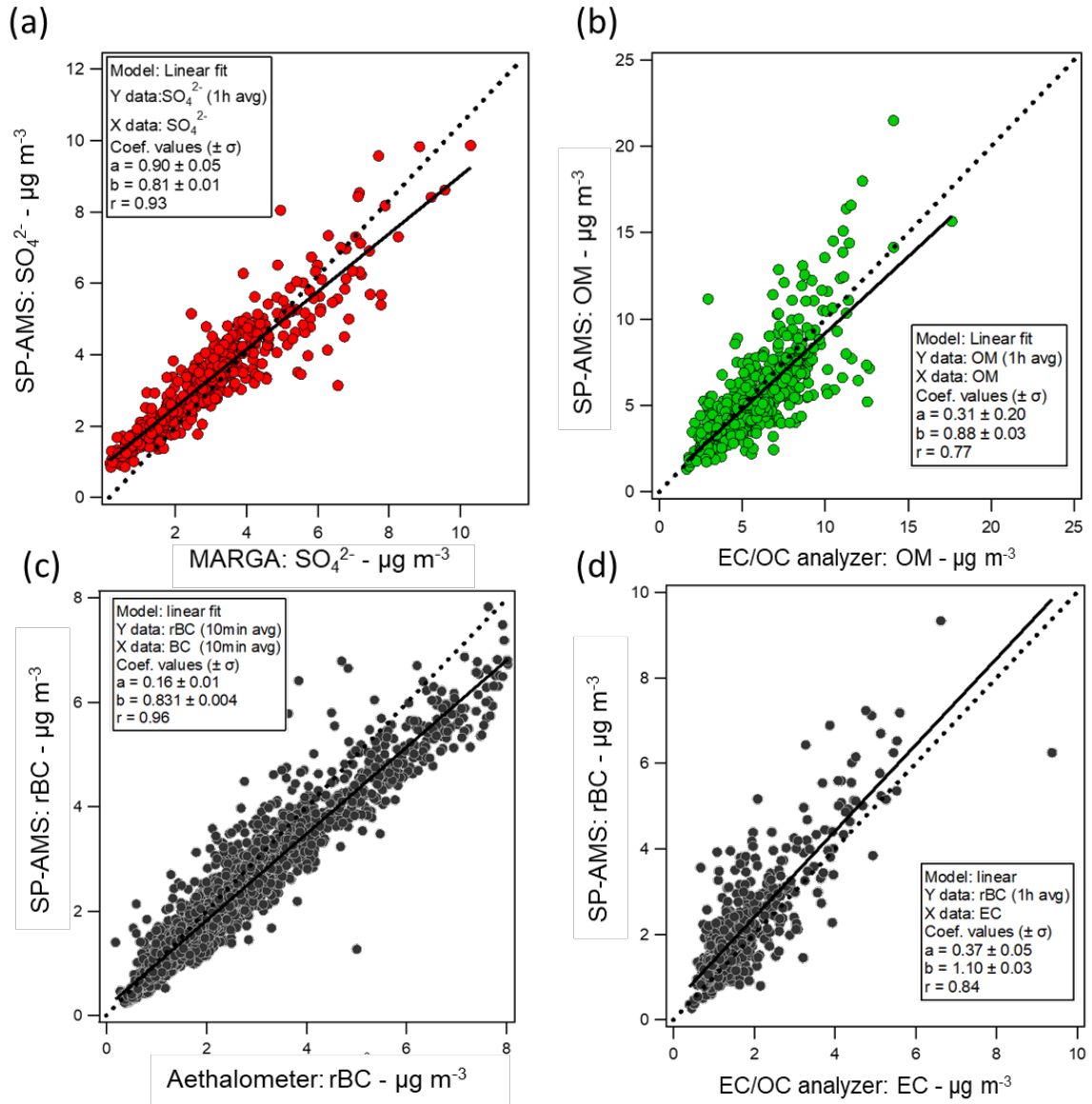
Figure S3: Scatter plots of (a) the hourly-averaged SO_4^{2-} mass concentration measured by the SP-AMS and MARGA, (b) and the hourly-averaged OA and OM (estimated from OC concentration using a 2.2 conversion factor) mass concentrations measured by the SP-AMS and OC/EC analyser, respectively. Comparisons of 10-min averaged rBC mass concentrations measured by the SP-AMS with (c) BC and (d) EC mass concentrations measured by the aethalometer and OC/EC analyser, respectively.
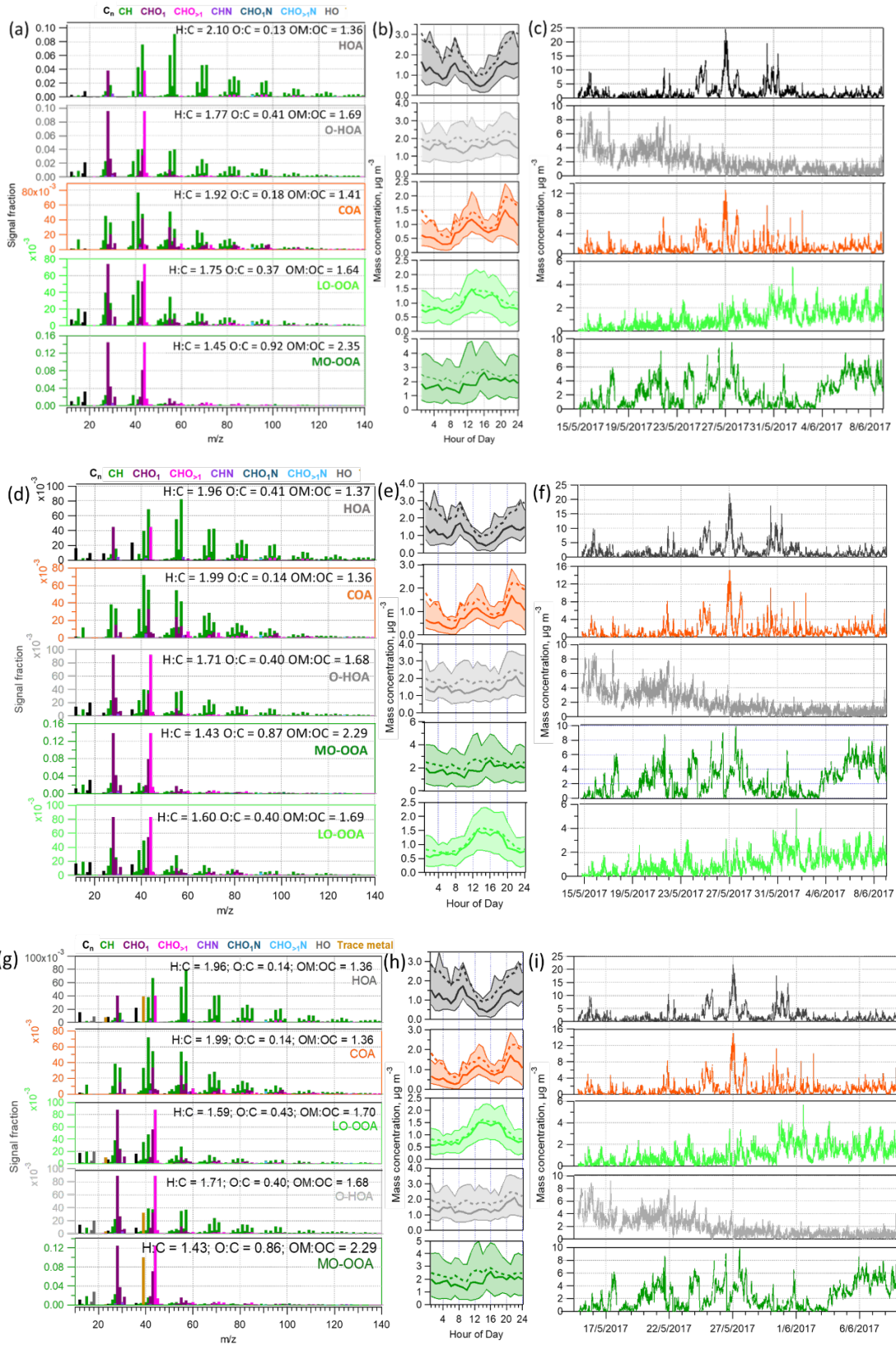
Figure S4: Mass spectra, diurnal variations (median - plain line, mean – dotted line, 25th and 75th centiles - shaded area) and time series of PMF factors obtained from the laser-on measurements. (a-c) OA only, (d-f) OA and rBC fragments (C_n^+: C_1^+-C_9^+), and (g-i) OA, C_n^+ and metal ions were used as the PMF inputs.
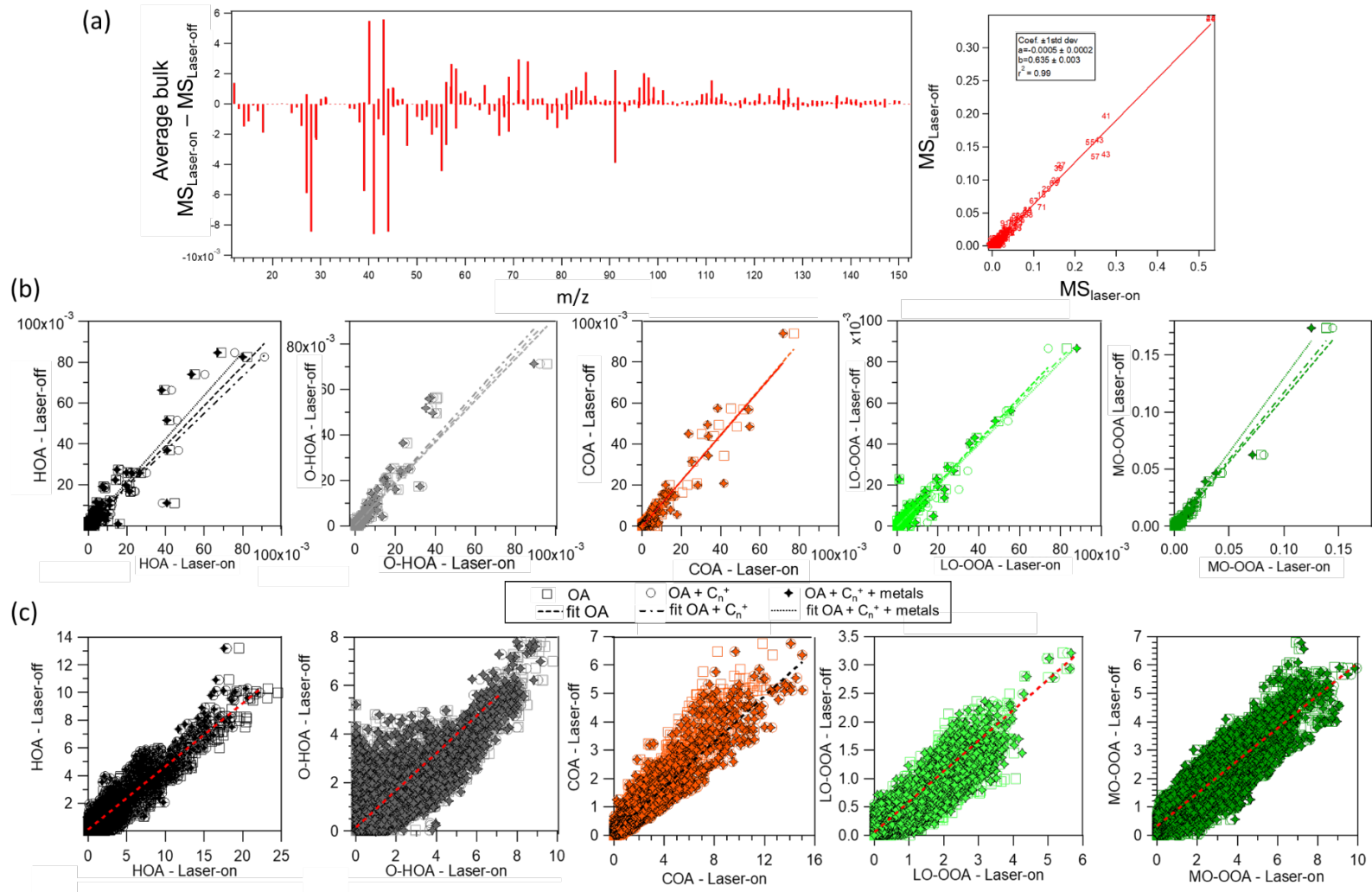
Figure S5: (a) Mass spectral difference (left) and scatter plot (right) of the averaged total organics between laser-off and laser-on (including C_n^+) measurements. Comparisons of (b) mass spectra and (c) time series of individual OA component obtained from the PMF analysis of laser-off and laser-on measurements (OA only, OA + C_n^+, OA + C_n^+ + metal as PMF inputs).
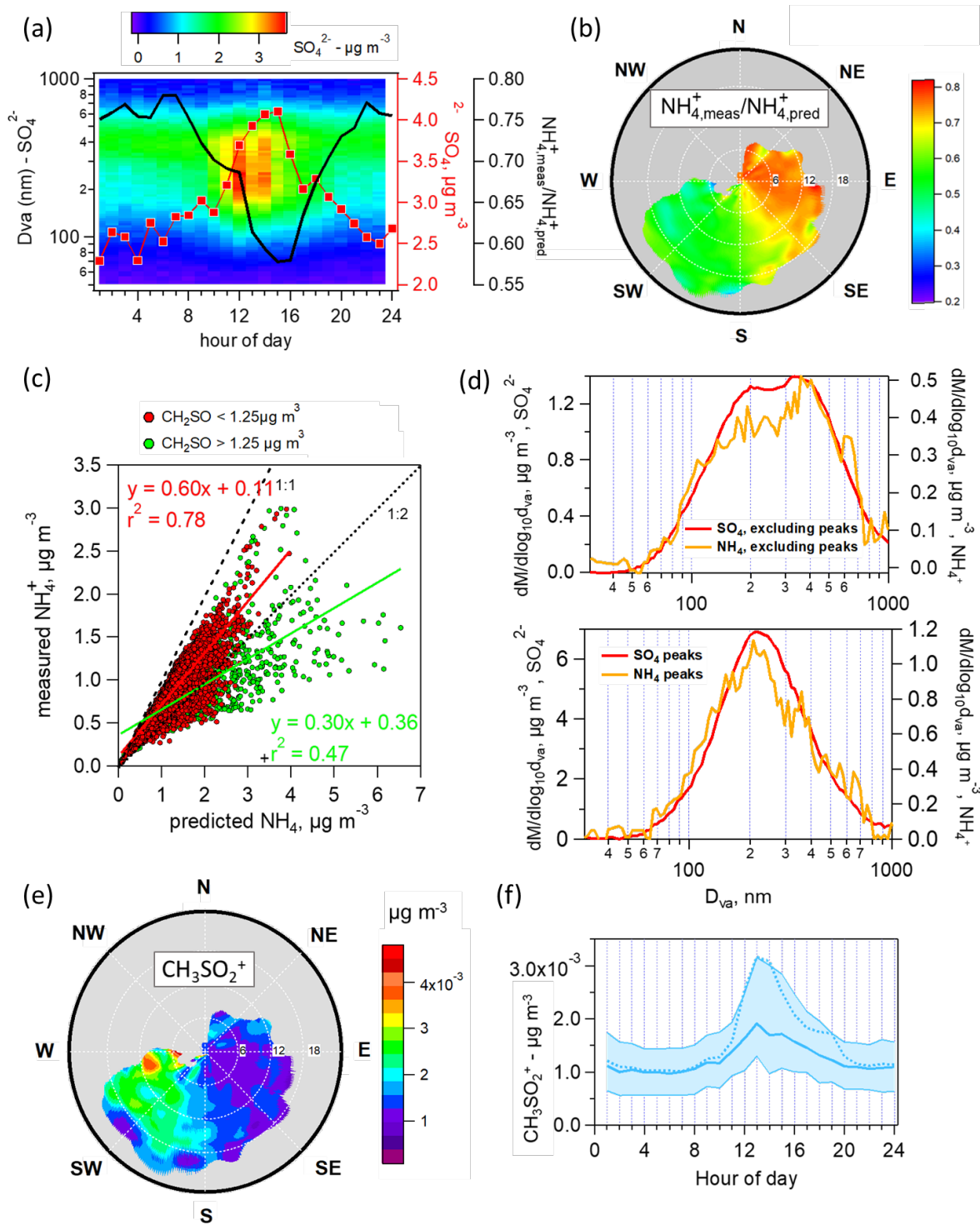
Figure S6: (a) Diurnal cycles of SO_4^{2-} size distribution, SO_4^{2-} mass concentrations and measured to predicted NH_4^+ ratios. (b) NWR graph of measured to predicted NH_4^+ ratios, (c) Comparison between measured and predicted NH_4^+ for data associated to CH_2SO^+ mass concentrations > 1.25 µg m^{-3} (red) and < 1.25 µg m^{-3} (green). (d) Size distributions of SO_4^{2-} and NH_4^+ for data associated to SO_4^{2-} mass concentrations < 7 µg m^{-3} (top) and > 7 µg m^{-3} (bottom). (e) NWR graph and (f) diurnal cycle of $CH_3SO_2^+$ fragment in µg m^{-3} (median - plain line, mean – dotted line, 25th and 75th centiles - shaded area).
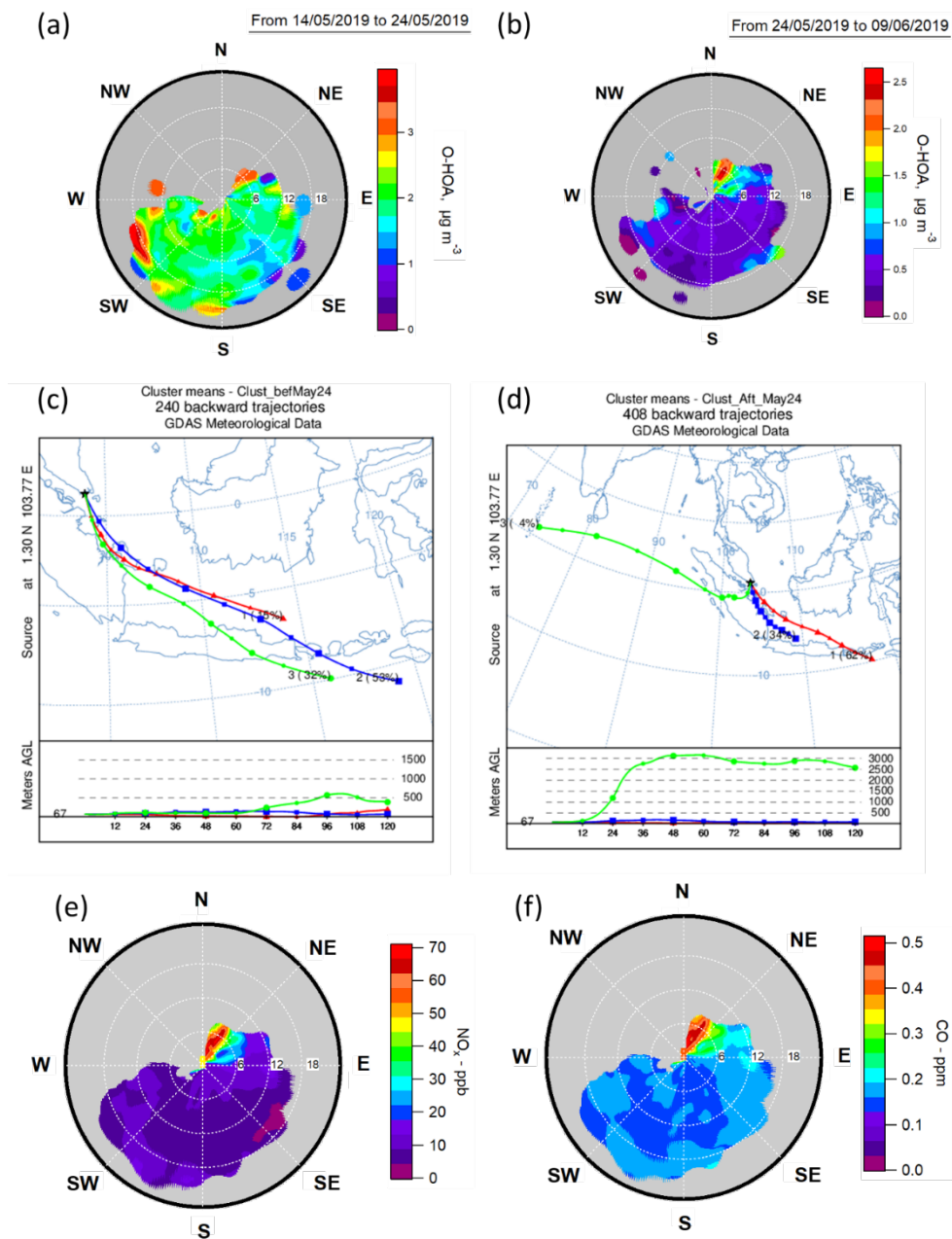
Figure S7: NWR graph of O-HOA (a) before and (b) after May 24th 2017. Results of cluster analysis of 120 h back-trajectories obtained (c) before and (d) after May 24th 2017. NWR graph of (e) NO_x and (f) CO during the whole sampling period.
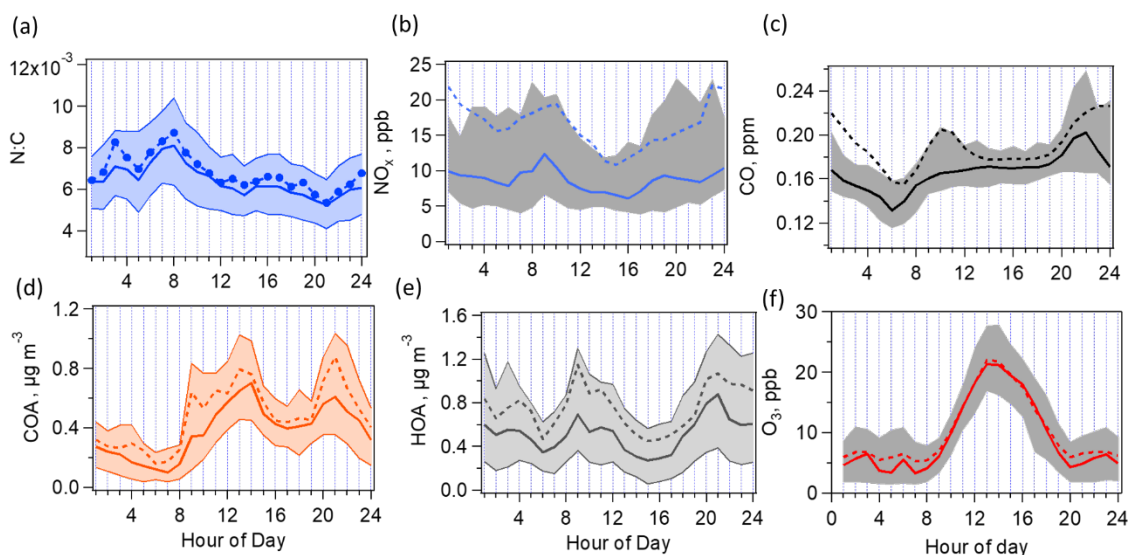
Figure S8: Diurnal cycles of (a) N:C (laser-off mode), (b) NO_x, (c) CO, (d) COA, (e) HOA, and (f) O_3 over the campaign. The plain and dotted lines represent the medians and averages values, respectively. The shaded regions represent the 25th and 75th percentiles. Note that data between May 25th to 28th were excluded for HOA and COA due to the strong unknown emission during the nighttime.
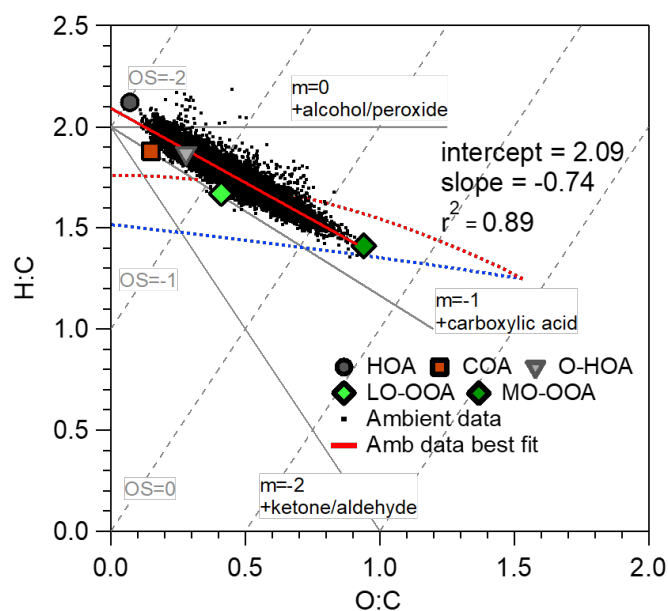
Figure S9: Elemental ratios of ambient data and PMF factors (coloured symbols) determined by the improved-ambient elemental ratio analysis based on the method outlined in Canagaratna et al., (2015).
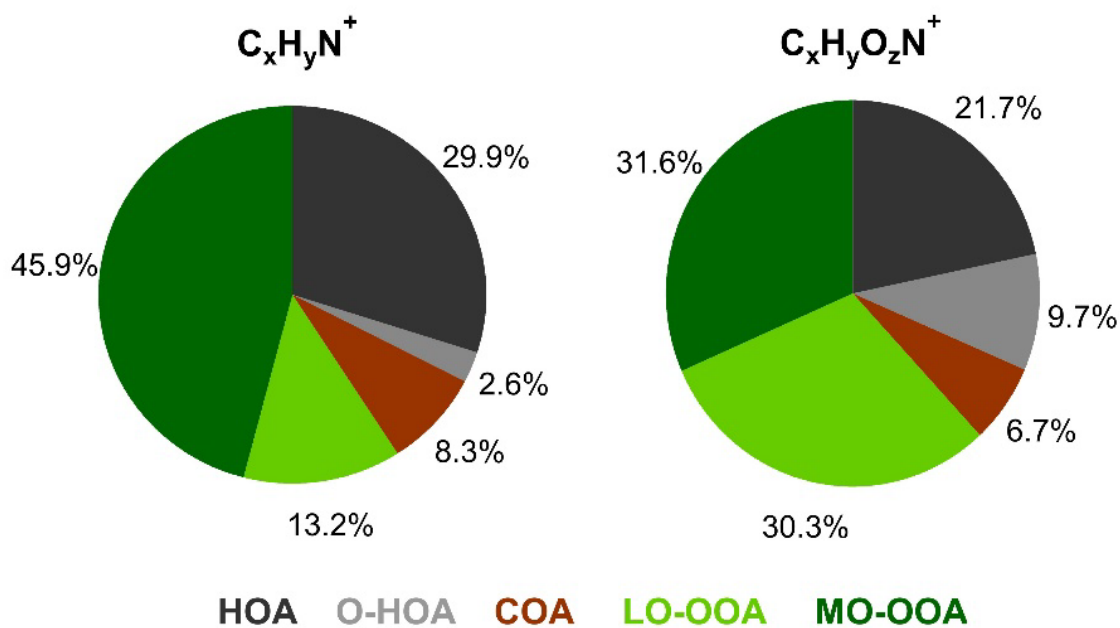
Figure S10: Contributions of each OA factor to the N-containing fragment groups (Kasthuriarachchi et al., (2020)).
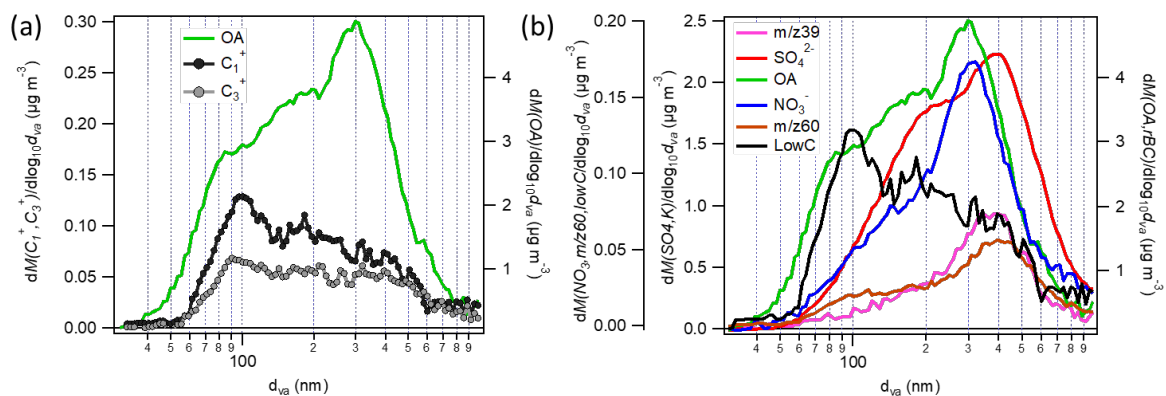
Figure S11: (a) Size distributions of (a) m/z 12 (C_1^+), m/z 36 (C_3^+), and OA measured by the laser-on mode. (b) Size distributions of lowC (i.e., sum of C_1^+, C_2^+ and C_3^+), OA, SO_4^{2-}, NO_3^-, m/z 39 (surrogate for K^+), and m/z 60 measured by the laser-on mode. Similar size distribution of m/z 60 and m/z 39 (K^+) are observed.
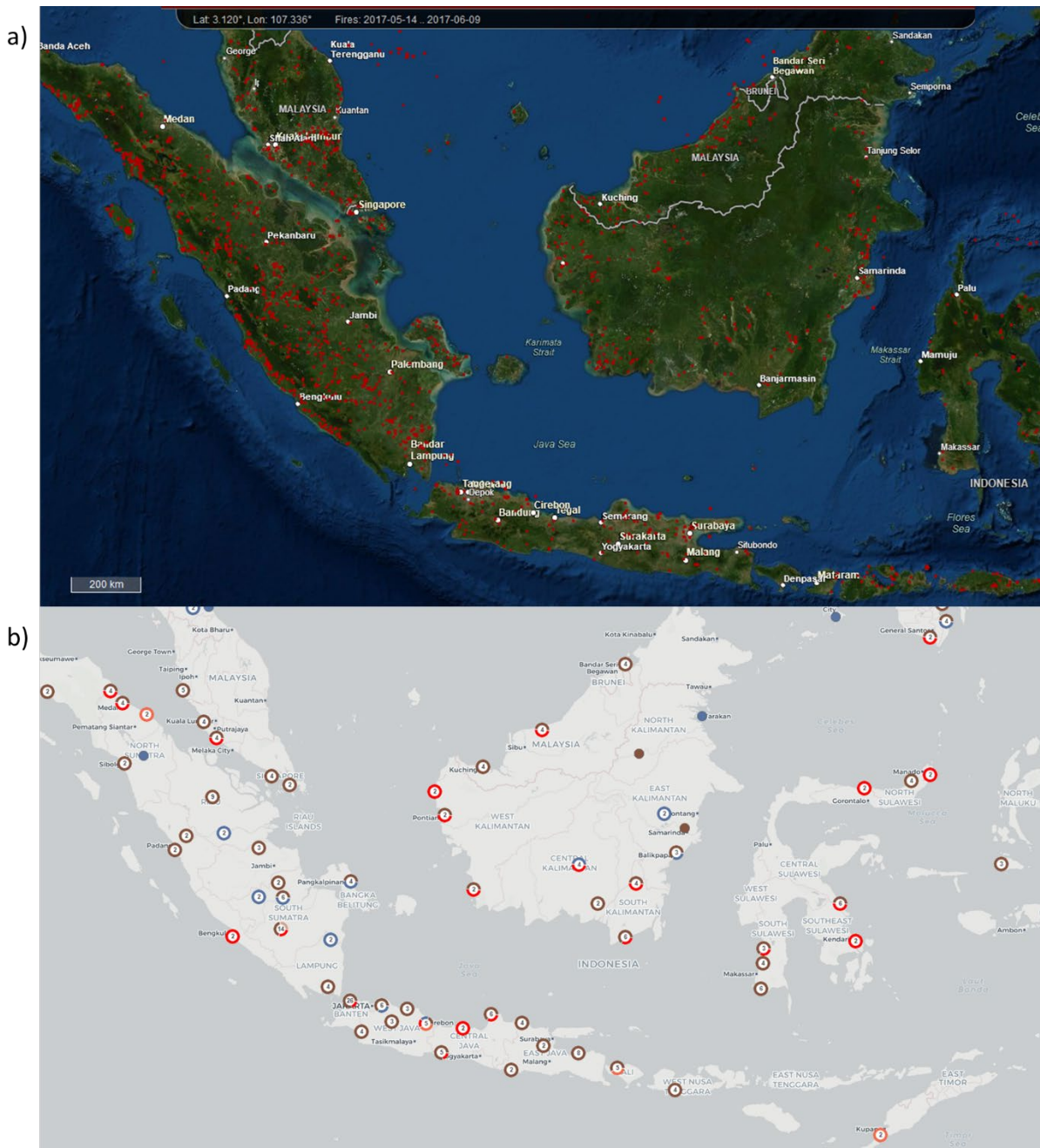
Figure S12: (a) Map of fire events identified by the Modis Active fire products over the whole campaign (https://firms.modaps.eosdis.nasa.gov/, © 2013 ESRI, i-cubed, GeoEye). (b) Locations of coal power plants in the surrounding countries (e.g., Malaysia and Indonesia). The power plant statuses are indicated by different colour: red – in construction, brown – operating, salmon – permitted, and blue – shelved (https://endcoal.org.tracker/, data: Global Energy Monitor, ©OpenStreetMap, ©CARTO).
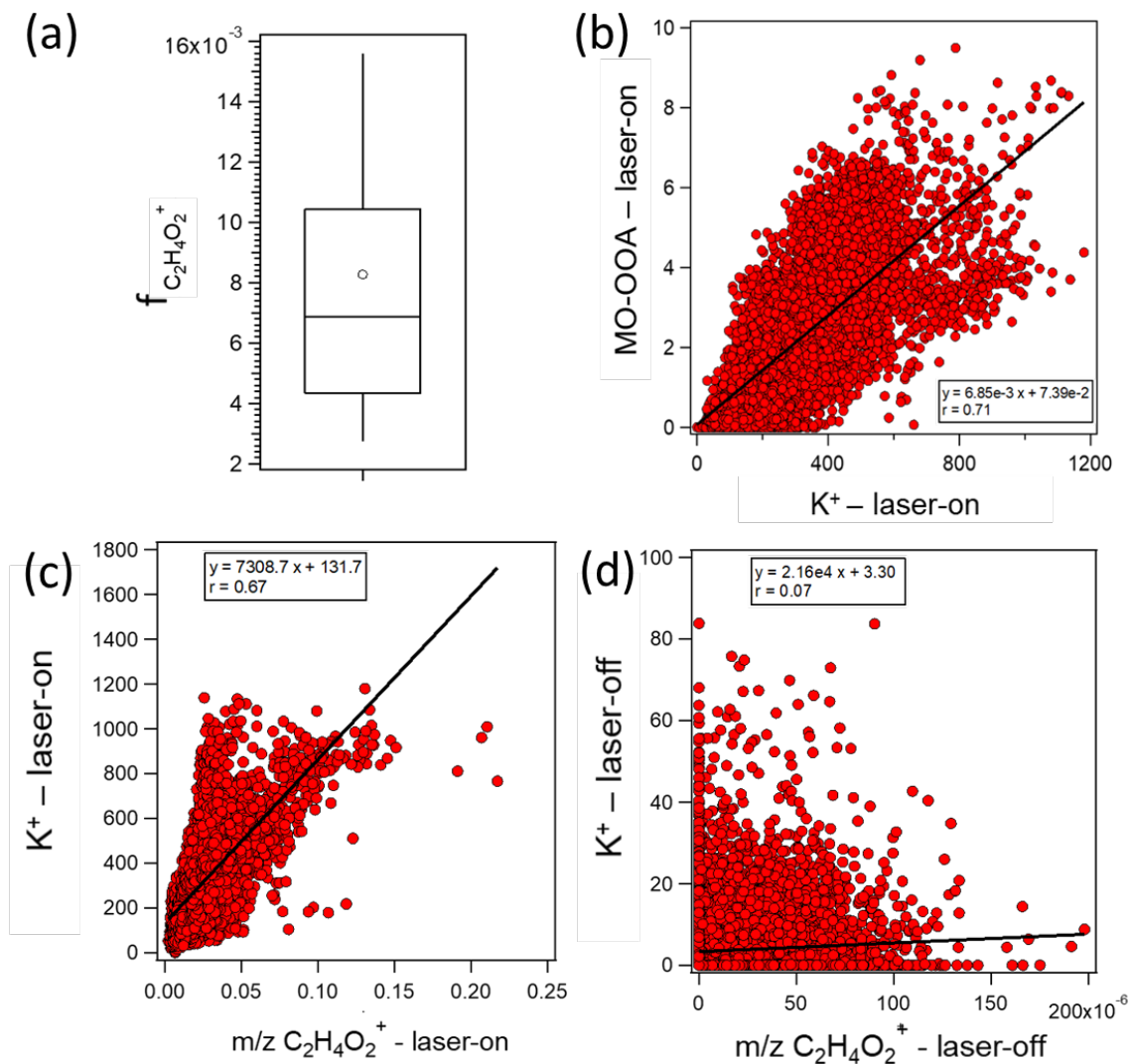
Figure S13: (a) Box plots of $f_{C2H4O2+}$ (5th, 25th, 50th, 75th and 95th percentiles). The average is indicated by the marker (open circle). Scatter plots of (b) MO-OOA vs. K^+ signals obtained by the laser-on mode, (c) K^+ signals vs. m/z $C_2H_4O_2^+$ signals obtained by the laser-on mode, and (d) K^+ signals vs. m/z $C_2H_4O_2^+$ signals obtained by the laser-off mode.
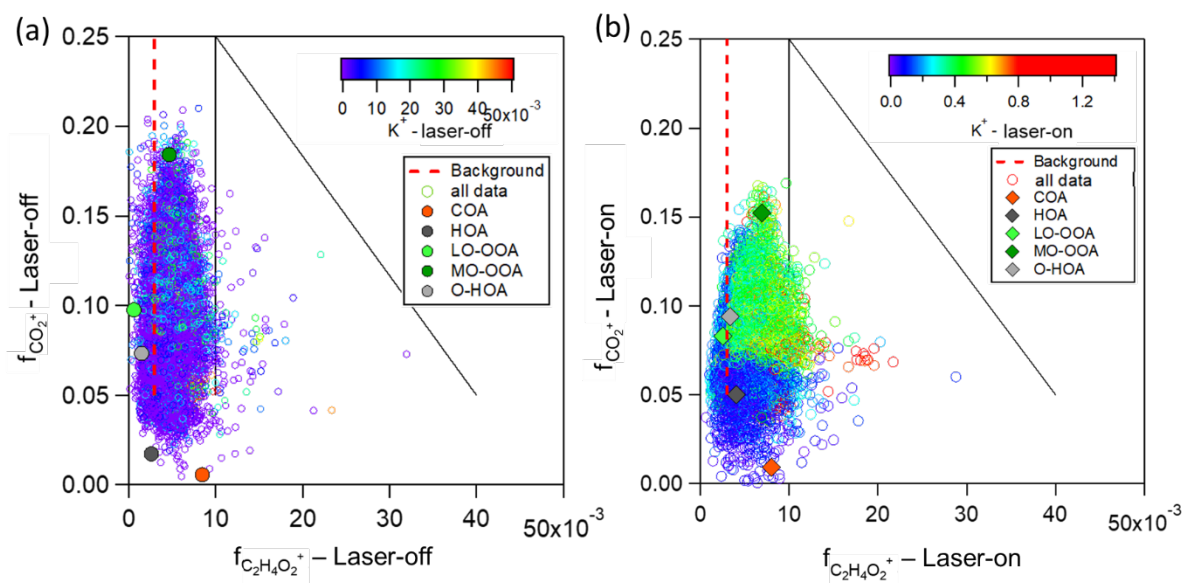
Figure S14: Scatter plots of f_{CO2+} vs. $f_{C2H4O2+}$, The symbols are colored by potassium (K^+) ion intensities based on (a) the laser-off mode, and (b) the laser-on mode measurements (Dash red line – 0.3% background value, and plain black lines define the space with and without significant biomass burning influence (i.e., inside and outside the triangular region, respectively, Cubison et al., (2011)).

Figure S15: PSCF graphs of (a) K^+, (b) Rb^+ and (c) m/z $C_2H_4O_2^+$ signals. NWR plots of (d) K^+, (e) Rb^+, (f) m/z $C_2H_4O_2^+$, (g) Ni^+, (h) V^+, and (i) Na^+, measured by the laser-on mode of SP-AMS measurements during the whole campaign.

5

Table S1: List of industrial plants and power stations located in Jurong Island (i.e., the industrial zone in the southwest direction of the sampling site).

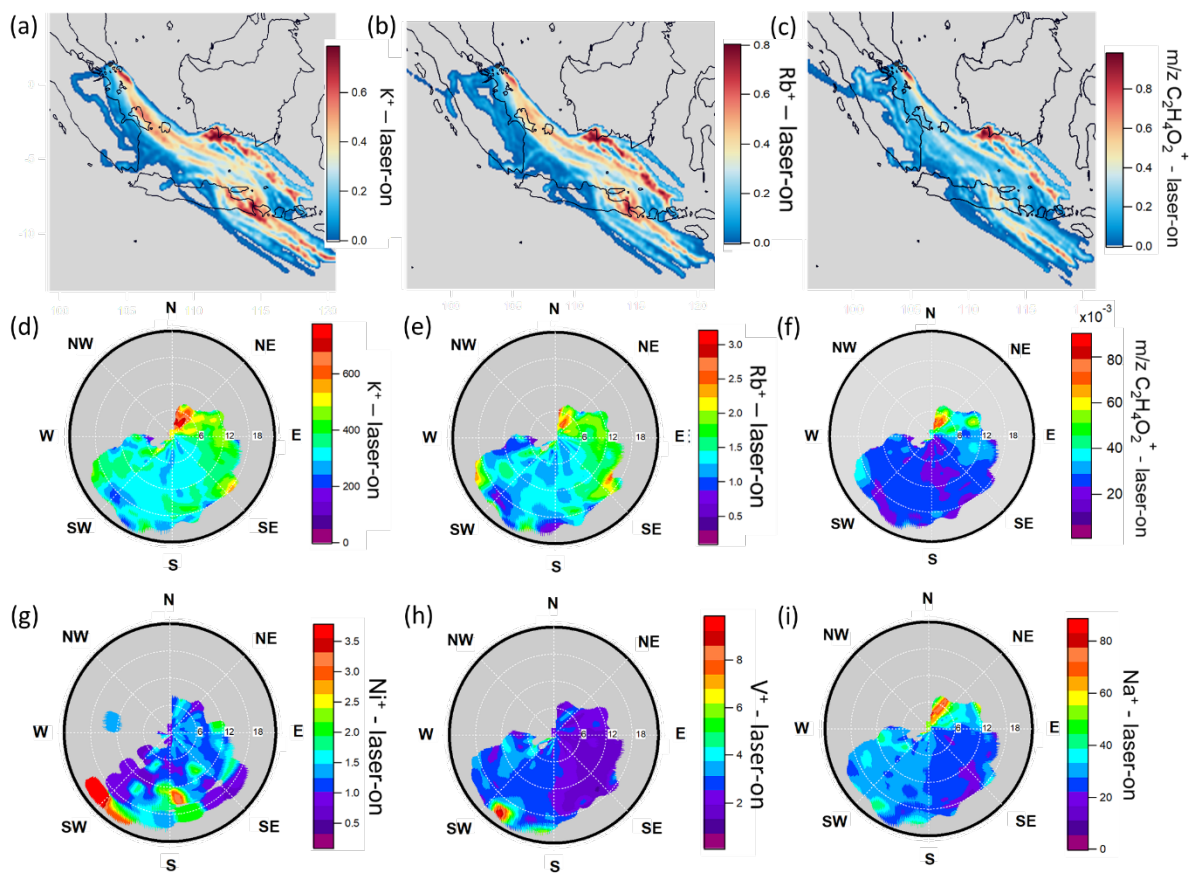| Industry	Activity	Products	Sources
LANXESS	Chemical plant	Inorganic pigments, organic leather chemicals, chrome tanning salts, ion exchange resins, reverse osmosis membrane products, antimicrobial active ingredients, preservatives and disinfectants, etc.	http://lanxess.sg/
Afton Chemical	Chemical plant	Manufactures petroleum additives, including driveline, engine oil, fuel and industrial additives	https://www.aftonchemical.com/
BASF	Chemical plant	Solvents, amines, resins, glues, electronic-grade chemicals, industrial gases, basic petrochemicals, inorganic chemicals, thermoplastics, foams and urethanes	https://www.basf.com/sg/en.html
BP plc	Petroleum Company		https://www.bp.com/en/global/corporate/what-we-do/bp-worldwide/bp-in-singapore.html
Celanese	Chemical plant	Acetic acid, vinyl acetate ethylene polymers	https://www.chemicals-technology.com/projects/celanese/
Evonik	Chemical plant	Feed additives, lubricant additives, hydrogen peroxide, precipitated and fumed silica, acrylic resins, monomers, moulding compounds and high-performance polymers	https://aps.evonik.com/region/seaanz/en/company/seaanz/singapore/
ExxonMobil	Refinery and chemical plant	Engine and heavy-duty vehicles oils (e.g., low-sulphur diesel, jet fuel) and industrial/specialty lubricants	https://www.exxonmobil.com.sg/Company/Overview/Who-we-are/Singapore-Chemical-Plant
DuPont de Nemours Inc.	Chemical plant	Nylon resin cubes for the automotive, electronics and appliance industries	https://www.dupont.com.sg/
Mitsui Chemicals	Chemical plant	Methyl styrene	https://www.azbil.com/case/aac/app_004/app_004a.html
Mitsui Elastomer	Chemical plant	High-performance elastomers	
Chevron Oronite	Energy and chemical plant	Oils, lubricants additives	https://www.chevron.com/worldwide/singapore
Petrochemical Complex of Singapore	Petrochemical plant	Ethylene, propylene, acetylene, butadiene, 1-butene, MTBE, benzene, toluene and xylene	https://www.spc.com.sg/
Singapore Petroleum Company Ltd	Petrochemical plant	Oils, lubricant additives	
Shell	Petrochemical plant	Ethylene oxide, styrene monomers, propylene oxide, polyols	https://www.shell.com.sg/about-us/projects-and-sites/shell-jurong-island.html

Stepan Company	Chemical plant	Polymers, surfactants	https://www.stepan.com/why-stepan/manufacturing_strengths.aspx
The Polyolefin Company	Chemical plant	Plastics, polyethylene, polymers and polymer additives	https://www.tpc.com.sg/
Chevron Philips	Chemical plant	High Density Polyethylene	http://www.cpchem.com/en-us/company/loc/Pages/Jurong-Island.aspx
Sumitomo Chemical	Chemical plant	Absorbent Polymers	https://www.sumitomo-chem.com.sg/regional_presence/singapore/
Pulau Seraya Power station	Power station	Oil, Natural gas, combined heat and power	https://ytlpowerseraya.com.sg/
PacificLight	Power station	Natural gas	https://www.pacificlight.com.sg/
Tembusu Multi-Utilities Complex	Power station	Biomass Clean Coal energy production	https://www.tuaspower.com.sg/tembusu-multi-utilities-complex/
Sembcorp Cogen	Power station	Natural gas	https://www.sembcorp.com/en/
Keppel Merlimau Cogen	Power station	Oil, natural gas and combined heat and power, coal gasification for feedstock production	http://www.kepinfra.com/en/content.aspx?sid=4259

Table S2: Averages and standard deviations of metal ions measured by the laser-on mode of SP-AMS for the entire period of the campaign. Limits of detection (LOD) were determined using the particle-free air (i.e., ambient air passed through an inlet filter).

Signal (Hz)	K^+	Na^+	Rb^+	V^+	Ni^+
LOD	36.09	22.21	0.82	0.33	0.66
Mean	335.82	31.62	1.29	2.28	0.48
Standard deviation	210.63	24.87	1.05	2.38	0.61

Table S3: Correlation coefficients (r) and slopes of linear regression between PMF factors determined by the laser-off and laser-on mode. Three additional PMF scenarios were conducted for the laser-on mode measurements (i.e., including (1) OA only, (2) OA and C_n^+, and (3) OA, C_n^+, and metals ions in the PMF input matrix).

PMF factors		HOA		COA		O-HOA		LO-OOA		MO-OOA	
		MS	TS	MS	TS	MS	TS	MS	TS	MS	TS
OA	Slope	0.98	0.44	1.12	0.50	0.91	0.61	1.05	0.54	1.13	0.62
	R	0.95	0.95	0.98	0.94	0.95	0.85	0.97	0.94	0.99	0.92
OA + C_n^+	Slope	0.99	0.46	1.11	0.41	0.94	0.59	1.01	0.53	1.17	0.58
	R	0.91	0.92	0.95	0.92	0.95	0.80	0.98	0.92	0.99	0.91
OA + C_n^+ + metal	Slope	1.06	0.45	1.11	0.40	0.97	0.58	0.99	0.50	1.30	0.58
	R	0.93	0.91	0.95	0.94	0.95	0.78	0.99	0.93	0.99	0.91

Table S4: Comparisons of the PMF results obtained from different CDCE correction approach (Pre-CDCE: PMF solution obtained by the CDCE-corrected input matrices, Post-CDCE: PMF solution corrected by CDCE). The post-CDCE solutions represent the corresponding base cases reported in the main text, Figure 3, and Figure S4.

PMF factors	LO-OOA			MO-OOA			COA			O-HOA			HOA		
Laser status	OFF	ON		OFF	ON		OFF	ON		OFF	ON		OFF	ON	
Type of PMF	OA	$+ C_n^+$	$+ C_n^+ +$ metal	OA	$+ C_n^+$	$+ C_n^+ +$ metal	OA	$+ C_n^+$	$+ C_n^+ +$ metal	OA	$+ C_n^+$	$+ C_n^+ +$ metal	OA	$+ C_n^+$	$+ C_n^+ +$ metal
Contribution to total OA mass (%)															
Post-CDCE	10.4	12.6	13.1	32.1	24.5	26.7	11.7	14.6	15.4	26.4	22.2	22.0	19.4	23.7	22.8
Pre-CDCE	12.4	12.3	12.1	30.8	28.5	29.6	12.6	16.3	17.8	21.0	20.6	19.7	23.2	22.2	21.4
Contribution to total rBC mass (%)															
Post-CDCE	NA	29.2	30.1	NA	6.2	6.4	NA	1.3	1.4	NA	20.1	20.7	NA	43.1	44.4
Pre-CDCE	NA	29.9	31.5	NA	7.4	8.8	NA	1.8	2.3	NA	26.5	24.4	NA	34.4	33.0
C_1^+/C_3^+															
Post-CDCE	NA	0.81	0.79	NA	0.54	0.29	NA	NA	NA	NA	1.00	1.00	NA	0.66	0.65
Pre-CDCE	NA	0.88	0.85	NA	1.76	1.57	NA	NA	NA	NA	0.90	0.89	NA	0.63	0.62
Time series - correlation coefficient (r)															
Post- vs. Pre-CDCE	0.98	0.97	0.91	0.99	0.99	0.99	0.98	0.97	0.96	0.89	0.93	0.94	0.99	0.97	0.97
Time series – slope															
Post- vs. Pre-CDCE	1.17	1.06	1.06	0.96	0.99	1.09	1.07	0.86	0.83	0.81	1.05	1.11	1.27	1.04	1.10
Normalized mass spectra - correlation coefficient (r)															
Post- vs. Pre-CDCE	1.00	0.95	0.94	1.00	1.00	0.99	1.00	0.93	0.92	1.00	0.99	0.99	0.97	0.99	0.99

References

Canagaratna, M. R., Jimenez, J. L., Kroll, J. H., Chen, Q., Kessler, S. H., Massoli, P., Hildebrandt Ruiz, L., Fortner, E., Williams, L. R., Wilson, K. R., Surratt, J. D., Donahue, N. M., Jayne, J. T. and Worsnop, D. R.: Elemental ratio measurements of organic compounds using aerosol mass spectrometry: characterization, improved calibration, and implications, Atmos Chem Phys, 15(1), 253–272, doi:10.5194/acp-15-253-2015, 2015.

Cubison, M. J., Ortega, A. M., Hayes, P. L., Farmer, D. K., Day, D., Lechner, M. J., Brune, W. H., Apel, E., Diskin, G. S., Fisher, J. A., Fuelberg, H. E., Hecobian, A., Knapp, D. J., Mikoviny, T., Riemer, D., Sachse, G. W., Sessions, W., Weber, R. J., Weinheimer, A. J., Wisthaler, A. and Jimenez, J. L.: Effects of aging on organic aerosol from open biomass burning smoke in aircraft and laboratory studies, Atmos Chem Phys, 11(23), 12049–12064, doi:10.5194/acp-11-12049-2011, 2011.

Kasthuriarachchi, N. Y., Rivellini, L.-H., Adam, M. G. and Lee, A. K. Y.: Strongly absorptive primary and secondary brown carbon in an urban, under review, Environ Sci Technol, 2020.

Middlebrook, A. M., Bahreini, R., Jimenez, J. L. and Canagaratna, M. R.: Evaluation of Composition-Dependent Collection Efficiencies for the Aerodyne Aerosol Mass Spectrometer using Field Data, Aerosol Sci. Technol., 46(3), 258–271, doi:10.1080/02786826.2011.620041, 2012.

Willis, M. D., Lee, A. K. Y., Onasch, T. B., Fortner, E. C., Williams, L. R., Lambe, A. T., Worsnop, D. R. and Abbatt, J. P. D.: Collection efficiency of the soot-particle aerosol mass spectrometer (SP-AMS) for internally mixed particulate black carbon, Atmos Meas Tech, 7(12), 4507–4516, doi:10.5194/amt-7-4507-2014, 2014.